Limit Cycle Oscillations in High Performance Robot Drives

Wallenborg, Anders; Åström, Karl Johan

1988

Document Version:
Publisher's PDF, also known as Version of record

CODEN: LUTFD2/(TFRT-7376)/1-16/(1988)

Limit Cycle Oscillations in High Performance Robot Drives

Anders Wallenborg
Karl-Johan Åström

Department of Automatic Control
Lund Institute of Technology
January 1988

Department of Automatic Control
Lund Institute of Technology
P.O. Box 118
S-221 00 Lund Sweden

Document name
Report

Date of issue
January 1988

Document Number
CODEN: LUTFD2/(TFRT-7376)/1-16/(1988)

Author(s)
Anders Wallenborg and Karl-Johan Åström

Supervisor

Sponsoring organisation

Title and subtitle
Limit cycle oscillations in high performance robot drives.

Abstract

Analysis and design of high performance robot drives require that elastic modes and nonlinear friction are considered. A control law based on linear state feedback and an observer can be used to provide active damping of the resonant modes. The achievable bandwidth is limited by the appearance of limit cycle oscillations at zero speed. The limit cycles are caused by the Coulomb friction in the drive motor, and their appearance is related to the stability of the regulator. It is shown that an unstable linear regulator is a sufficient condition for limit cycle oscillations in this type of system. This, in combination with the inherent windup problem, leads to the conclusion that unstable regulators should be avoided when designing flexible servo control systems. The stability of the regulator depends mainly on a dimensionless quantity, which includes the load inertia, the spring constant of the elastic modes and the closed loop natural frequency. Analytic expressions have been derived from which approximate values of the stability limit can be calculated with good accuracy. All results have been verified experimentally on a simple prototype system.

Key words

Classification system and/or index terms (if any)

Supplementary bibliographical information

ISSN and key title

ISBN

Language
English

Number of pages
16

Recipient's notes

Security classification

Paper presented at the International Conference
'Control 88', University of Oxford, UK,
13-15 April 1988.

LIMIT CYCLE OSCILLATIONS IN HIGH PERFORMANCE ROBOT DRIVES

Anders Wallenborg and Karl Johan Åström

Department of Automatic Control,
Lund Institute of Technology, Lund, Sweden

Abstract

Analysis and design of high performance robot drives require that elastic modes and nonlinear friction are considered. A control law based on linear state feedback and an observer can be used to provide active damping of the resonant modes. The achievable bandwidth is limited by the appearance of limit cycle oscillations at zero speed. The limit cycles are caused by the Coulomb friction in the drive motor, and their appearance is related to the stability of the regulator. It is shown that an unstable linear regulator is a sufficient condition for limit cycle oscillations in this type of system. This, in combination with the inherent windup problem, leads to the conclusion that unstable regulators should be avoided when designing flexible servo control systems. The stability of the regulator depends mainly on a dimensionless quantity, which includes the load inertia, the spring constant of the elastic modes and the closed loop natural frequency. Analytic expressions have been derived from which approximate values of the stability limit can be calculated with good accuracy. All results have been verified experimentally on a simple prototype system.

1. Introduction

Elastic modes in gears and harmonic drives are characteristic features of current robot drives. Elasticities are also becoming more common due to the trend towards lighter mechanical designs. The elastic modes are lightly damped, and depend on configuration and load. The control system must therefore provide active damping in high performance robot drives. Improved performance also requires that nonlinearities, such as Coulomb friction, are considered in the design.

Several authors have studied flexible servo systems and nonlinear friction compensation in rigid body servo systems. See for example [1], [3] and [9]. We believe, however, that the combined effects of flexible modes and nonlinear friction have not yet been fully investigated. This paper has been motivated by observations of limit cycle oscillations in flexible servo systems [11]. The mechanism which generates the oscillations is explained. The oscillations are due to a combination of elasticity, nonlinear friction and demands for high performance of the system. In this paper we present mathematical models, analysis and experimental results.

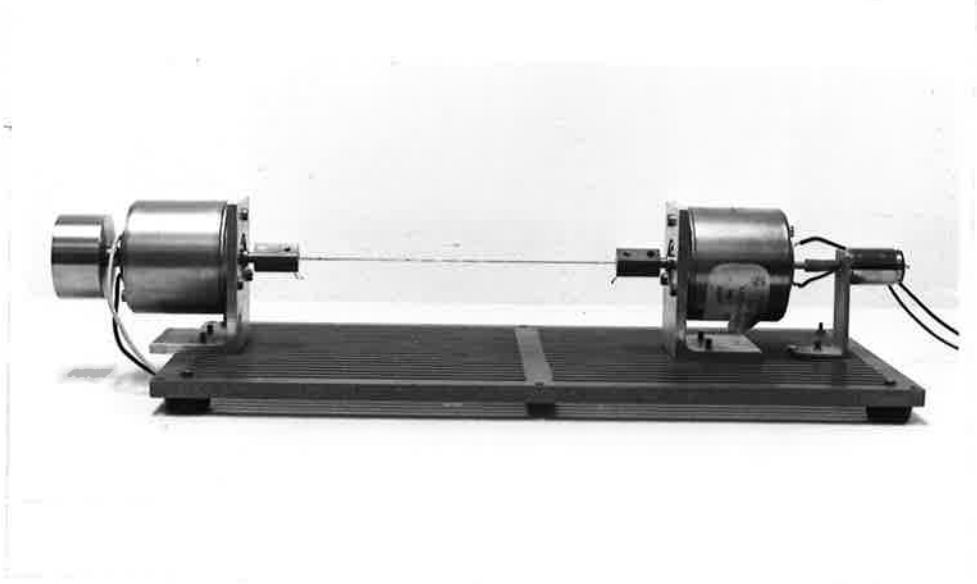

Figure 1. The experimental setup. The DC drive motor and tacho generator are to the right, and the inertial load is to the left.

2. Experimental setup

A robot joint can be modelled as a two-inertia system, with a drive motor coupled to an inertial load via an elastic spring representing flexible modes. A laboratory model has been built to experimentally verify the results. It consists of an electric DC drive motor connected to an inertial load by a weak shaft. In order to keep the instrumentation simple, we have studied the speed control problem only. A 'colocated' speed sensor is assumed. The measured signal is thus the drive motor speed. This is normally case in robotic applications. The physical dimensions of the system were chosen such that the resonance frequency of the oscillatory modes would be reasonably low. This was accomplished by using a thin wire for the weak shaft. A photograph of the experimental setup is shown in Figure 1.

3. Robot Joint Model

Linear model

Let the variables related to the drive motor have index 1 and the variables related to the load have index 2. The moments of inertia of the drive motor and load are J_1 and J_2, respectively. The spring constant is denoted k, and the spring damping coefficient is d. Viscous friction in bearings etc. is described by two damping coefficients d_1 and d_2. See Figure 2. The drive motor is assumed to give a torque M proportional to the input voltage u, hence $M = k_m u$. This is a good approximation for a motor with current feedback.

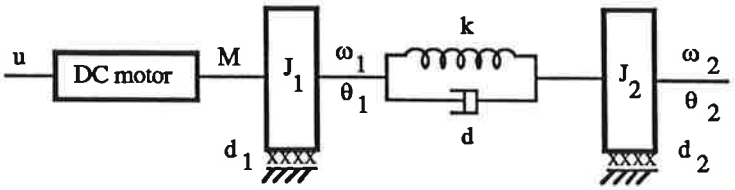

Figure 2. Linear robot joint model.

Introduce the state variables $x_1 = \omega_1, x_2 = \omega_2$, and $x_3 = \theta_2 - \theta_1$, where ω_1 and ω_2 are the angular velocities of drive motor and load, and θ_1 and θ_2 are the corresponding angular positions. The measured output signal is $y = k_{\omega_1}\omega_1$ [Volt], where k_{ω_1} is the drive motor tachometer gain. The input signal u is the input voltage to the drive amplifier. Torque balances for the motor and load give the following state space model:

$$\dot{x}(t) = \begin{pmatrix} -\frac{d_1+d}{J_1} & \frac{d}{J_1} & \frac{k}{J_1} \\ \frac{d}{J_2} & -\frac{d_2+d}{J_2} & -\frac{k}{J_2} \\ -1 & 1 & 0 \end{pmatrix} x(t) + \begin{pmatrix} \frac{k_m}{J_1} \\ 0 \\ 0 \end{pmatrix} u(t) \tag{1}$$

$$y(t) = \begin{pmatrix} k_{\omega 1} & 0 & 0 \end{pmatrix} x(t)$$

Using the parameter values from the experimental system, the following linear state space model is obtained:

$$\dot{x}(t) = \begin{pmatrix} -0.45 & 0 & 109 \\ 0 & -0.07 & -16.0 \\ -1 & 1 & 0 \end{pmatrix} x(t) + \begin{pmatrix} 1136 \\ 0 \\ 0 \end{pmatrix} u(t) \tag{2}$$

$$y(t) = \begin{pmatrix} 0.1 & 0 & 0 \end{pmatrix} x(t)$$

Note that the damping d is negligible. The state space model (2) has the transfer function

$$G_1(s) = \frac{113.6(s^2 + 0.07s + 16)}{(s+0.1)(s^2 + 0.4s + 125)} \tag{3}$$

Simplified linear model

The elements of the system matrix that contain damping are very small, cf. eqn (1) and (2). A simplified state space model can be obtained by neglecting the damping terms, i.e. $d = d_1 = d_2 = 0$. This gives

$$\dot{x}(t) = \begin{pmatrix} 0 & 0 & \frac{k}{J_1} \\ 0 & 0 & -\frac{k}{J_2} \\ -1 & 1 & 0 \end{pmatrix} x(t) + \begin{pmatrix} \frac{k_m}{J_1} \\ 0 \\ 0 \end{pmatrix} u(t) \tag{4}$$

$$y(t) = \begin{pmatrix} k_{\omega 1} & 0 & 0 \end{pmatrix} x(t)$$

This simplified model can be used for approximate analytical calculations.

Nonlinear model including static friction

A more detailed robot joint model, including Coulomb friction, has been used for simulation. The Coulomb friction is modelled as two friction torques M_{fi}, $(i = 1, 2)$, acting on the motor and load [1], [2]:

$$M_{fi} = \begin{cases} -F_i \operatorname{sign}(\omega_i) & (\omega_1 \neq 0) \\ -M_i & (\omega_1 = 0 \text{ and } |M_i| < F_i) \\ -F_i \operatorname{sign}(M_i) & (\omega_1 = 0 \text{ and } |M_i| > F_i) \end{cases} \tag{5}$$

The parameter F_i is the magnitude of the friction torque and M_i is the total torque acting the shaft (excluding the nonlinear friction). For simplicity the friction model (5) is symmetric, i.e. the friction torque is the same in both directions of rotation.

The magnitude of the friction torques were estimated by measuring the input voltage required to run the system in steady state at lowest possible speed. At low speed, the viscous friction torques can be neglected. The input signal is then proportional to the sum of the Coulomb friction on the motor and the load. The estimated friction torque values were $F_1 = F_2 = 5 \cdot 10^{-4}$ Nm.

4. Linear Control Design

The linear model (2) has two poorly damped oscillatory modes with the natural frequency $\omega_o = 11.2$ rad/s, and one slow real pole at $s = -0.12$. The control design is based on pole placement with state feedback and an observer [6]. The control law is

$$\begin{cases} \dot{\hat{x}} = A\hat{x} + Bu + K(y - C\hat{x}) \\ u = l_r y_r - L\hat{x} \end{cases} \tag{6}$$

where $\hat{x}$ is the estimated state vector. The feedback gain L is chosen to give the desired closed loop poles, and l_r is chosen to give unit steady state gain from the reference value y_r to the process output. As a *nominal design* the closed loop poles are all placed at approximately the same distance from the origin as the resonant open loop poles. The selected closed loop natural frequency is $\omega_{cl} = 12$ rad/s. The resonant poles are moved to a well-damped location (relative damping $\zeta = 0.7$).

The observer design is a trade-off between convergence rate and noise sensitivity. The observer gain K is chosen such that the observer poles are placed in the same pattern as the closed loop system, but at a distance $\alpha\omega_{cl}$ from the origin. The factor α is given the nominal value $\alpha = 1.5$, which implies that initial state estimate errors will decay faster than the closed loop dynamics.

Controller stability and windup protection

The design method above does not guarantee that the resulting controller is stable. Eliminate u from the observer equation in (6), and collect all terms on the right hand side containing the state vector estimate $\hat{x}$:

$$\begin{cases} \dot{\hat{x}} = (A - BL - KC)\hat{x} + Bl_r y_r + Ky \\ u = l_r y_r - L\hat{x} \end{cases}$$

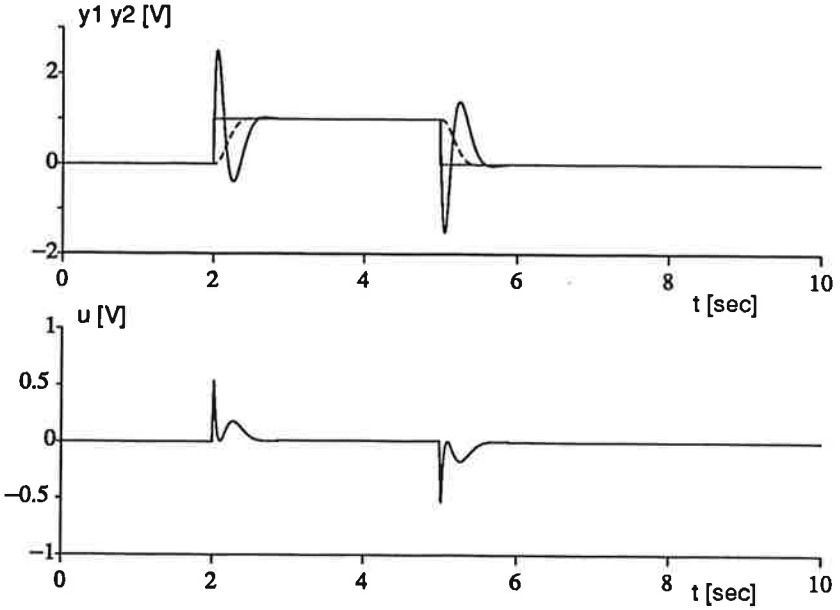

Figure 3. Closed loop step response with linear model. Nominal control design ($\omega_{cl} = 12$). Solid line = motor speed, dashed line = load speed.

The controller is unstable if the matrix $(A - BL - KC)$ has eigenvalues in the right half of the plane. This is the case with the nominal design. It is an undesired property, which implies that extra precautions must be taken in the implementation to avoid windup problems during startup, or if the loop is at any time broken.

Simulation results

The closed loop step response was simulated with SIMNON [4], [5]. The reference step amplitude, $y_r = 1$ V, was selected to keep the maximum torsion of the weak shaft within given bounds. In the simulations with the nonlinear joint model, a non-zero initial condition $\omega_1(0) = 1.0$ rad/s was used to emulate small initial start-up disturbances.

The step response with the linear model and nominal control design is shown in Figure 3. Note that the drive motor speed y_1 has a significant overshoot, whereas the step response of the load, y_2, has a well damped closed loop step response. The reason for this is that the open loop transfer functions from the input u to y_1 and y_2 have different zeros.

The closed loop step response with the nonlinear model including Coulomb friction (cf. Section 3) is shown in Figure 4. A limit cycle oscillation appears when the reference value is zero. By simulating the closed loop system with the Coulomb friction on either the drive motor or the load set to zero, it was found experimentally that the oscillations are caused by the nonlinear friction in the drive motor. The oscillations appear only when the speed reference is zero. This can be explained by the discontinuity in the Coulomb friction at zero speed. At non-zero speed values, the Coulomb friction can be regarded as a constant load disturbance. Hence it does not influence the stability of the system as long as the direction of rotation does not change. It causes a steady state error, however, since the control law does not have integral action. The limit cycle oscillation can be eliminated by reducing the specified closed loop

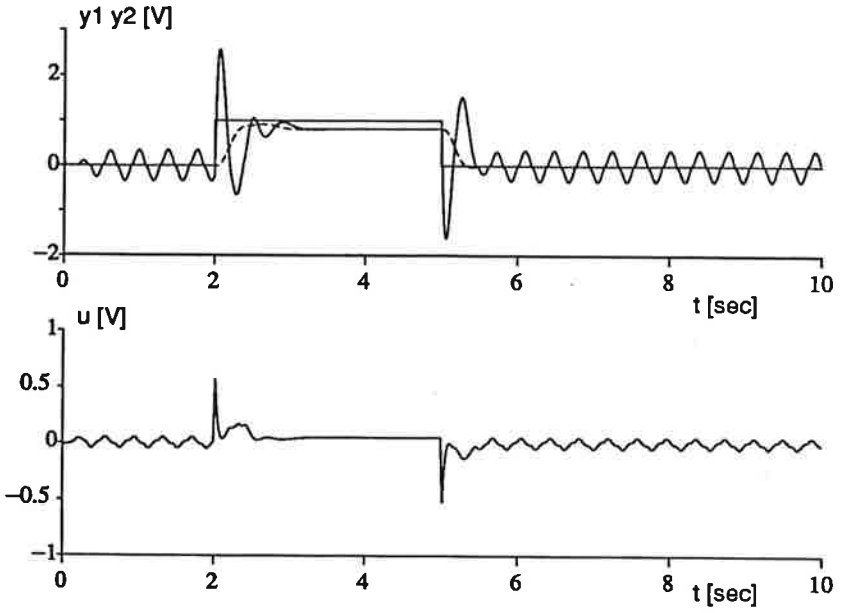

Figure 4. Closed loop step response with nonlinear model. Nominal control design ($\omega_{cl} = 12$). Solid line = motor speed, dashed line = load speed.

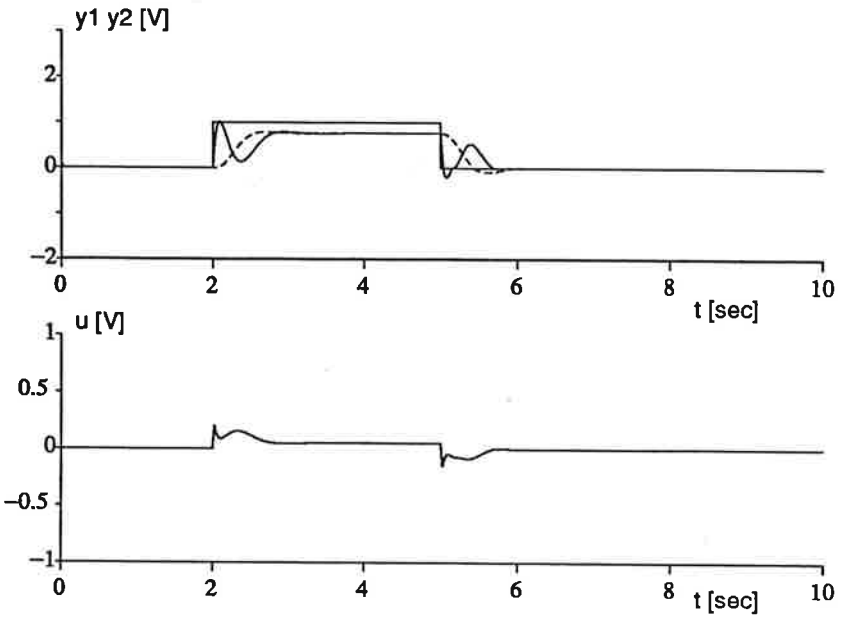

Figure 5. Closed loop step response with nonlinear model. Reduced bandwidth design ($\omega_{cl} = 8$). Solid line = motor speed, dashed line = load speed.

bandwidth. This is shown in Figure 5, which corresponds to a control design with $\omega_{cl} = 8$ rad/s.

5. Nonlinear Analysis

The behaviour described in Section 4 can be explained with the *describing function* method [2], [7], [10]. To apply this method, the system is decomposed

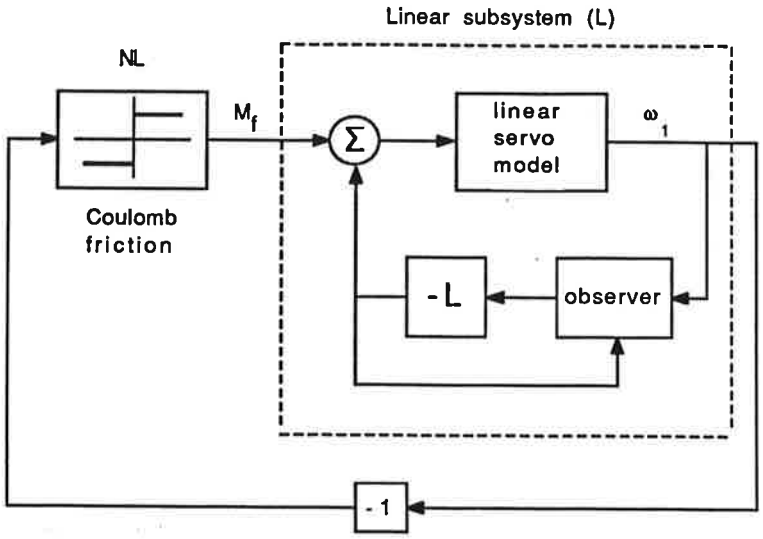

Figure 6. Servo system with speed control divided into linear and nonlinear subsystem.

into one linear and one nonlinear subsystem by neglecting the friction on the load, and approximating the Coulomb friction in the drive motor with an ideal relay function. To make the system autonomous, the speed reference y_r is zero. The decomposed system is shown in Figure 6.

The nonlinear friction torque M_f is modelled by

$$M_f = \begin{cases} +F, & (\omega < 0) \\ -F, & (\omega > 0) \end{cases} \tag{7}$$

where F is the magnitude of the Coulomb friction torque, cf. eqn (5). The describing function for (7) is

$$Y_N(C) = \frac{4F}{\pi C} \tag{8}$$

where C is the amplitude of the periodic oscillation. Note that the point $-1/Y_N(C)$ moves along the negative real axis with C. The Nyquist curve for the linear subsystem with nominal control design, i.e. $\omega_{cl} = 12$ rad/s, is shown in Figure 7. The Nyquist curve intersects the negative real axis at $G(j\omega) \approx -500$. The oscillation amplitude is given by

$$G(j\omega) = -\frac{1}{Y_N(C)} = -\frac{\pi C}{4F} \quad \Rightarrow \quad C = -\frac{4FG(j\omega)}{\pi} \tag{9}$$

With $F = 5{\cdot}10^{-4}$ Nm the amplitude is $C = 0.3$ Volt. The oscillation frequency is determined by the condition $\arg G(j\omega) = -180^o$, which in our case gives $\omega = 15.8$ rad/s. The absence of limit cycles with the lower bandwidth design ($\omega_{cl} = 8$ rad/s) is explained by the Nyquist curve (see Figure 8), which never intersects the negative real axis. Thus the describing function method predicts stability.

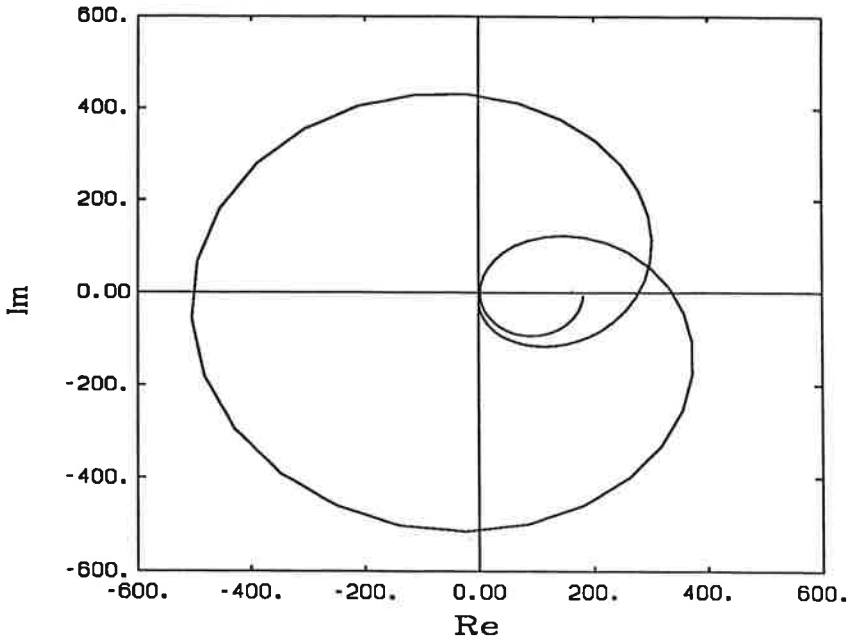

Figure 7. Nyquist curve for the linear subsystem in Figure 6 with $\omega_{cl} = 12$.

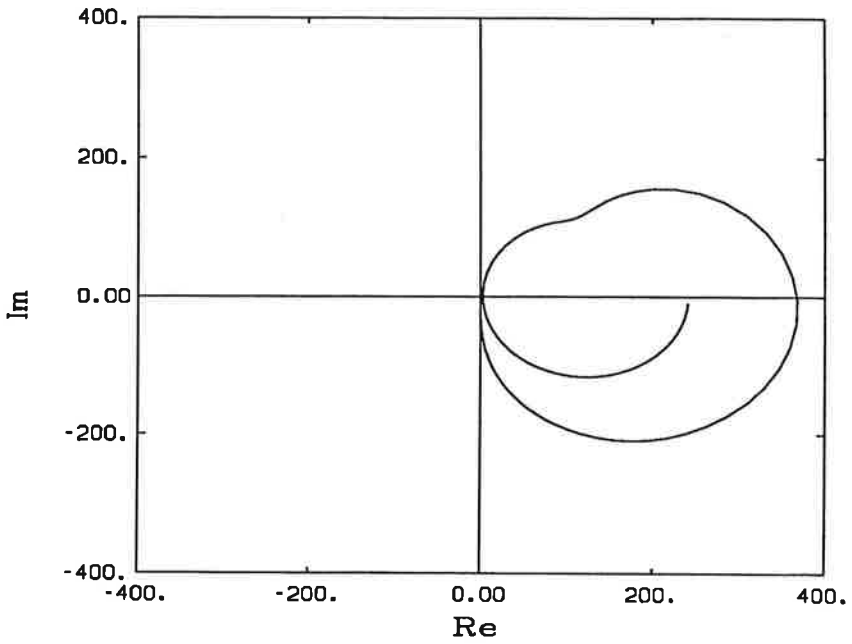

Figure 8. Nyquist curve for the linear subsystem in Figure 6 with $\omega_{cl} = 8$.

A sufficient condition for instability

The presence of limit cycles is related to the stability of the controller. An unstable controller is in fact a sufficient condition for limit cycles to appear according to the describing function method. To show this, we will first prove the following result.

LEMMA 1 Consider a system with a rational transfer function $G(s)$. Assume that the system is strictly proper, asymptotically stable and that the steady state gain $G(0)$ is finite and positive. Also assume that $G(s)$ has no zeros on

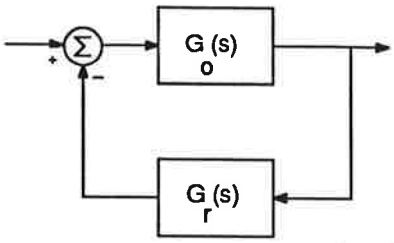

Figure 9. Block diagram of a linear system with a process $G_o(s)$ and a regulator $G_r(s)$ in the feedback loop.

the imaginary axis. Then the Nyquist curve $G(j\omega)$ must intersect the negative real axis if $G(s)$ has zeros in the right half plane.

Proof: Let the process transfer function be

$$G(s) = \frac{B(s)}{A(s)}$$

By assumption, the denominator $A(s)$ is stable i.e. it has all its zeros in the left half plane. Factor the numerator polynomial $B(s)$ as $B = B_1 B_2$, where B_1 has all its zeros in the right half plane and B_2 has all its zeros in the left half plane. Rewrite the transfer function $G(s)$ as

$$G(s) = \frac{B_1}{B_1^*} \cdot \frac{B_1^* B_2}{A} = G_1 \cdot G_2$$

where the zeros of B_1^* are the zeros of B_1 reflected in the imaginary axis. Notice that $G_1(j\omega)$ is an all-pass filter with unity gain. If $G(s)$ has zeros in the right half plane, then $\deg(B_1) > 0$ and the high frequency phase shift of $G_1(j\omega)$ is

$$\arg(G_1(j\omega)) = -n \cdot \pi + \epsilon$$

where $n = \deg(B_1)$ and $\epsilon \to 0$ as $\omega \to \infty$. The remaining part, G_2, of the transfer function G is minimum-phase and asymptotically stable. It is also strictly proper since $\deg(B_1^*) = \deg(B_1)$. Consequently, for high frequencies the phase shift of $G_2(j\omega)$ is

$$\arg(G_2(j\omega)) = -m\frac{\pi}{2} + \delta$$

where $m = \deg(A) - \deg(B)$ and $\delta \to 0$ as $\omega \to \infty$. Thus we can conclude that if $G(s)$ is non minimum-phase, then

$$\lim_{\omega \to \infty} \arg G(j\omega) = \phi_\infty = -(2n + m) \cdot \frac{\pi}{2} \leq \frac{-3\pi}{2}$$

In the absence of zeros on the imaginary axis, $\phi(\omega) = \arg G(j\omega)$ is a continuous function of ω. We know that $\phi(0) = 0$, since $G(s)$ is assumed to have a positive steady state gain, and that the asymptotic phase shift is $\phi_\infty \leq -3\pi/2$. Then there must exist a finite frequency ω_o such that $\phi(\omega_o) = -\pi$ and hence $G(j\omega)$ intersects the negative real axis at $\omega = \omega_o$. □

The linear part of the closed loop system (cf. Figure 6) has the structure shown in Figure 9, with one process and one controller block. The process

transfer function $G_o(s)$ from motor torque to motor speed is

$$G_o(s) = \frac{B_o(s)}{A_o(s)} = \frac{4544(s^2 + 0.07s + 16)}{(s + 0.1)(s^2 + 0.4s + 125)} \tag{10}$$

This transfer function is similar to (3). The only difference is in the steady state gain, since here we consider the motor torque as the input signal. With zero speed reference, the controller transfer function $G_r(s)$ can be calculated from (6):

$$G_r(s) = \frac{B_r(s)}{A_r(s)} = L(sI - A + BL + KC)^{-1}K \tag{11}$$

The closed loop transfer function is

$$G = \frac{B_o A_r}{A_o A_r + B_o B_r} = \frac{Q}{P} \tag{12}$$

Note that the controller poles appear as zeros in the closed loop system. The closed loop system is strictly proper, since $\deg(A_r) = \deg(A_o)$, $\deg(B_o) = \deg(A_o) - 1$ and $\deg(B_r) < \deg(A_r)$ (cf. eqn (12) above). The closed loop poles are always asymptotically stable (for any sensible control design !), and the complex zeros of $B_o(s)$ are in the left half plane. The closed loop steady state gain is positive, since a positive torque input will yield a positive speed output.

Now consider the case of an *unstable controller*. The transfer function $G(s)$ then has at least one zero, but no poles, in the right half plane. From Lemma 1 it can be concluded that the Nyquist curve of the closed loop linear subsystem must intersect the negative real axis. Assuming that the nonlinear friction can be modelled by an ideal relay function (7), the describing function method in combination with the Nyquist stability criterion predicts a limit cycle oscillation. This is a *sufficient but not necessary condition*, since the Nyquist curve may intersect the negative real axis even with a stable controller. It is conjectured from practical experience, however, that regulator instability is also a necessary condition for limit cycles to appear.

6. Performance Bounds

The regulator designed in Section 4 has the characteristic equation

$$A_r(s) = \det(sI - A + BL + KC) = 0 \tag{13}$$

where $A_r(s)$ is a third order polynomial

$$A_r(s) = s^3 + a_1 s^2 + a_2 s + a_3 \tag{14}$$

Assume a control design where all closed loop poles are placed at a distance ω from the origin and the complex poles have a relative damping ζ. The observer poles are placed in the same pattern but at a distance $\alpha\omega$ from the origin ($\alpha > 1$). Using the simplified linear model (4), the coefficients in $A_r(s)$ can be calculated as functions of the process and control design parameters. The errors introduced in the regulator poles by this simplification are quite small. Introducing the dimensionless quantity

$$\mathrm{w} = \frac{J_2\omega^2}{k} \tag{15}$$

the following coefficients of $A_r(s)$ were obtained with the symbolic manipulation program MACSYMA [8]:

$$\begin{aligned} a_1 &= \omega(2\zeta+1)(\alpha+1) \\ a_2 &= \frac{J_1 k}{J_2^2}\left(a_{20}\mathrm{w}^3 + a_{21}\mathrm{w}^2 + a_{22}\mathrm{w} + a_{23}\right) \\ a_3 &= \frac{J_1 k\omega}{J_2^2}\left(a_{30}\mathrm{w}^2 + a_{31}\mathrm{w} + a_{32}\right) \end{aligned} \tag{16}$$

where

$$\begin{aligned} a_{20} &= -\alpha^3 \\ a_{21} &= 4\alpha^2\zeta^2 + (2\alpha^3 + 4\alpha^2 + 2\alpha)\zeta - (\alpha^3 + \alpha^2 + \alpha) \\ a_{22} &= -\left(4\alpha\zeta^2 + (2\alpha^2 + 4\alpha + 2)\zeta + (\alpha^2 + \alpha + 1)\right) \\ a_{23} &= 1 + \frac{J_2}{J_1} \\ a_{30} &= \alpha^2(\alpha+1)(2\zeta+1) \\ a_{31} &= -\left(4\alpha(\alpha+1)(\zeta^2+\zeta) + \alpha^3 + \alpha^2 + \alpha + 1\right) \\ a_{32} &= (\alpha+1)(2\zeta+1)\left(1 + \frac{J_2}{J_1}\right) \end{aligned}$$

Regulator stability

The polynomial $A_r(s)$ is stable if

$$\begin{cases} a_1, a_2, a_3 > 0 \\ a_1 a_2 > a_3 \end{cases} \tag{17}$$

To evaluate the stability criterion $a_1 a_2 > a_3$, introduce the quantity e defined by

$$e = a_1 a_2 - a_3 \tag{18}$$

Inserting a_1, a_2 and a_3 from (16) into (18), simple but cumbersome calculations using (15) give

$$e = \frac{J_1\omega^3}{J_2}\left(c_0\mathrm{w}^2 + c_1\mathrm{w} + c_2\right) \tag{19}$$

where

$$\begin{aligned} c_0 &= -\alpha^3(\alpha+1)(2\zeta+1) \\ c_1 &= 8\alpha^2(\alpha+1)\zeta^3 + 4(\alpha^4 + 4\alpha^3 + 4\alpha^2 + \alpha)\zeta^2 \\ &\quad + 4(\alpha^4 + 2\alpha^3 + \alpha)\zeta + \alpha^4 + \alpha^3 + \alpha^2 + \alpha \\ c_2 &= -\left(8\alpha(\alpha+1)\zeta^3 + 4(\alpha^3 + 3\alpha^2 + 3\alpha + 1)\zeta^2\right. \\ &\quad \left. + 2(2\alpha^3 + 3\alpha^2 + 3\alpha + 2)\zeta + \alpha(\alpha+1)\right) \end{aligned}$$

The coefficient a_1 is always strictly positive, and does not influence stability. The sign of a_2 and e, however, will be negative for large w values. By calculating and plotting $a_2(\mathrm{w})$, $a_3(\mathrm{w})$ and $e(\mathrm{w})$ for a particular choice of design variables (ζ, α), we can get a more detailed picture of the set of w values for

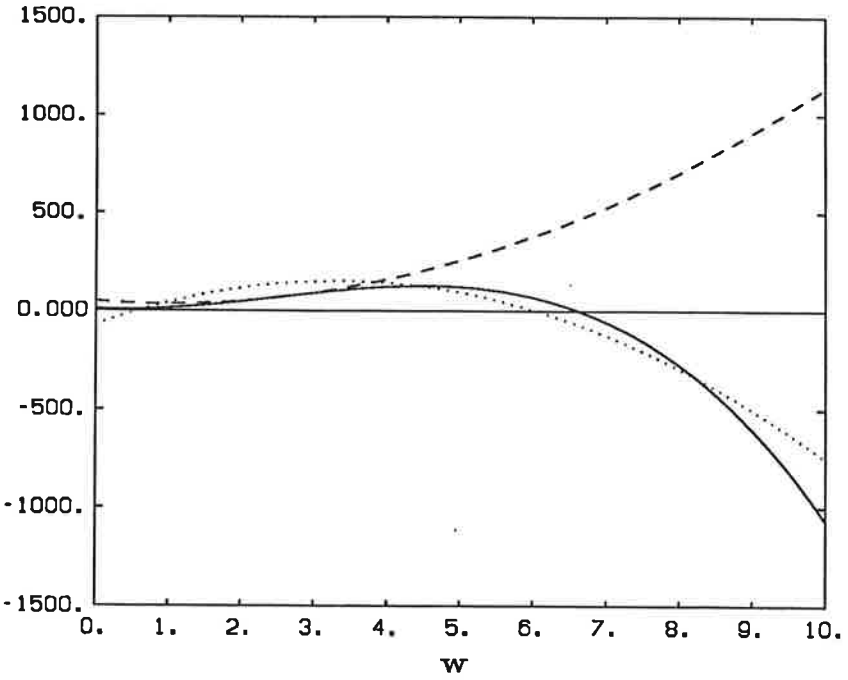

Figure 10. Normalized coefficients of the regulator characteristic polynomial. Nominal design case ($\omega = 12, \alpha = 1.5$). Solid line = $a_{2n}(\mathrm{w})$, dashed line = $a_{3n}(\mathrm{w})$ and dotted line = $e_n(\mathrm{w})$.

which the regulator is stable. Figure 10 shows a plot of the the normalized and dimensionless coefficients

$$a_{2n}(\mathrm{w}) = \frac{J_2^2}{J_1 k} a_2(\mathrm{w}); \qquad a_{3n}(\mathrm{w}) = \frac{J_2^2}{J_1 k \omega} a_3(\mathrm{w})$$

and

$$e_n(\mathrm{w}) = \frac{J_2}{J_1 \omega^3} e(\mathrm{w})$$

with nominal design parameters. The normalized coefficients are plotted because they are of the same order of magnitude and thus the sign shifts are more easily observed in the plot.

Bandwidth limit

The stability limit is in our case determined by the condition $e_n(\mathrm{w}) \leq 0$. The stable w interval is $0.59 < \mathrm{w} < 6.05$. With $J_2 = 150 \cdot 10^{-6}$ kgm^2 and $k = 2.4 \cdot 10^{-3}$ Nm/rad, the upper natural frequency limit corresponding to $\mathrm{w}_{max} = 6.05$ can be calculated from (15):

$$\omega_{max}^2 = \frac{k \mathrm{w}_{max}}{J_2} \quad \Rightarrow \quad \omega_{max} = 9.84 \text{ rad/s}$$

This is a good approximation of the true natural frequency limit. A numerical calculation of the regulator poles for different ω values using the complete servo model shows that the stability limit is $\omega_{max} = 9.90$ rad/s.

If a certain minimum closed loop natural frequency ω is required, the corresponding maximum inertial load J_2 (or, alternatively, the minimum k value) can be calculated from the w stability limit and (15). The influence of the

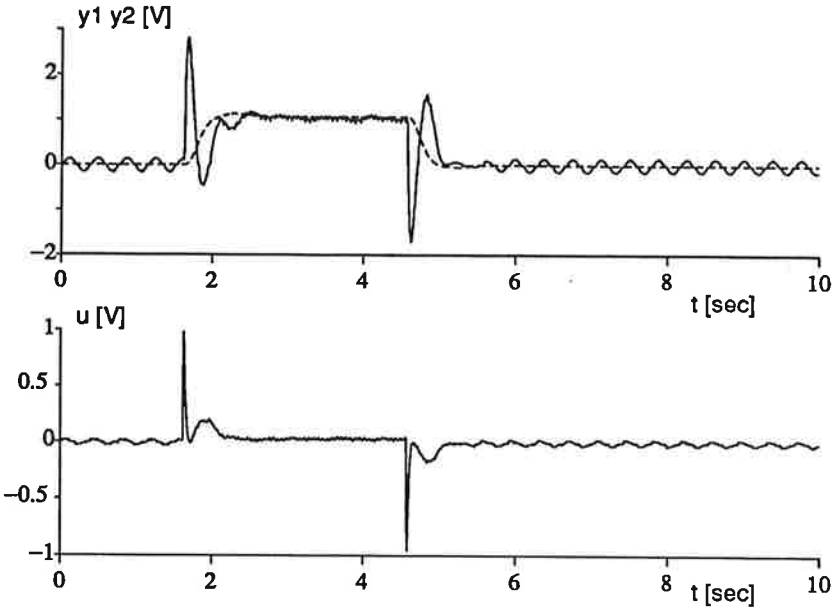

Figure 11. Measured closed loop step response with nominal design (ω_{cl} = 12 rad/s). Drive motor speed = solid line, load speed = dashed line.

control design on the achievable bandwidth can be investigated by plotting the normalized coefficients for different ζ and α values. By increasing the relative damping ζ of the closed loop system, the achievable bandwidth with respect to regulator stability is increased. A fast observer (increased α), on the other hand, has the opposite effect. Note that the sign of a_2 and a_3 depends not only on w, but also on the inertia ratio J_2/J_1. With reasonable inertia ratios this dependance is small, however, since J_2/J_1 only appears in the constant (w-independent) term.

7. Experimental Results

The continuous time control law (6) was implemented using conventional analog circuits with operational amplifiers. Before designing the circuits, the linear state space control law was transformed into a form suited for analog implementation by amplitude scaling of the state variables. The drive motor speed, the load speed, and the control signal u were logged using a data acquisition program with a sampling interval of 10 ms. A high frequency disturbance can be seen on the motor speed. It is caused by tachometer ripple, and the ripple frequency is proportional to the motor speed. The steady state speed (1 V = 10 rad/s) corresponds to a ripple frequency of 100 rad/s.

The experimental results agree well with the simulations. Limit cycle oscillations appear as predicted when the desired closed loop bandwidth is too high. Figure 11 shows the step response with the nominal (high bandwidth) design, and the step response with reduced bandwidth design (ω_{cl} = 8 rad/s) is shown in Figure 12. The frequency of the limit cycles measured in the experiments agrees well with the calculated value. The amplitude of the oscillation is approximately 0.2 V. This is smaller than the predicted value 0.3 V. The amplitude discrepancy can be explained by an incorrect value of the Coulomb friction torque. It follows from equation (9) that an incorrect value

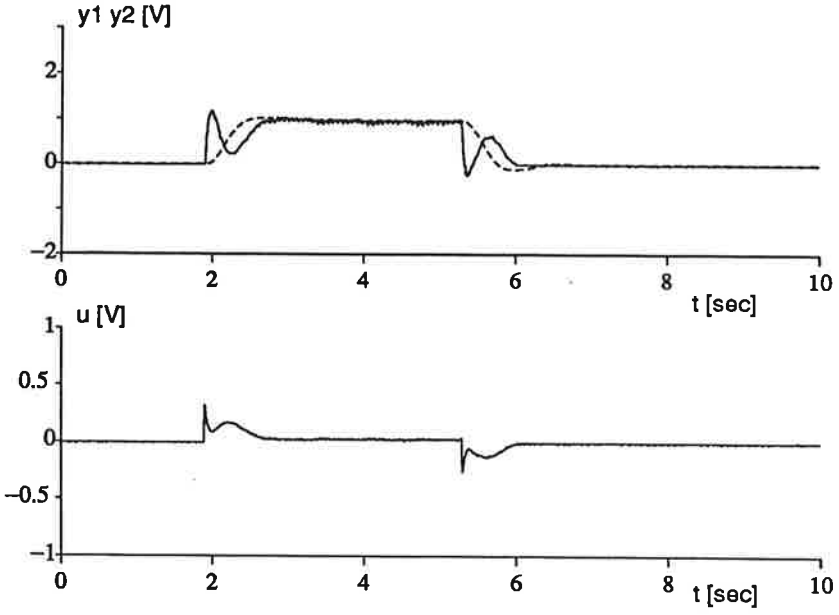

Figure 12. Measured closed loop step response with reduced bandwidth design ($\omega_{cl} = 8$ rad/s). Drive motor speed = solid line, load speed = dashed line.

of the friction torque gives an error in the predicted amplitude, but not in the frequency.

8. Conclusions

Simple mathematical models have been used to analyse and predict the behavior of a servo system with flexible modes and nonlinear friction. They give good insight into qualitative properties of the system, and also quite accurate quantitative results. A control law based on pole placement with linear state feedback and an observer can be used to provide active damping of the resonant modes in the system, provided that the poles are chosen appropriately. The achievable bandwidth is limited by the appearance of limit cycle oscillations at zero speed. The limit cycles are caused by the Coulomb friction in the drive motor, and their appearance is related to the stability of the regulator.

A sufficient condition for the appearance of limit cycles is that the linear regulator is unstable. The stability of the regulator depends on a dimensionless quantity w, which includes the load inertia, the spring constant of the elastic modes and the closed loop natural frequency. The regulator will be unstable for large w values and limit cycles appear. Analytic expressions have been derived from which approximate values of the stability limit can be calculated with good accuracy. The relation between unstable regulators and limit cycle oscillations, in combination with the inherent windup problem, indicates that unstable regulators should be avoided in control design for servo systems with elastic modes. The requirement that the regulator should be stable imposes constraints on the achievable bandwidth.

9. References

[1] ANWAR G., TOMIZUKA M., HOROWITZ R. and KUBO T. (1986): "Experimental Study on Discrete Time Adaptive Control of an Industrial Robot Arm," Proceedings of the 2nd IFAC Workshop on Adaptive Systems in Control and Signal Processing, July 1986. Lund Institute of Technology, Lund, Sweden.

[2] ATHERTON D. P. (1975): *Nonlinear Control Engineering*, (Student edition 1982), Van Nostrand Reinhold, Wokingham, Berkshire, England.

[3] CANUDAS DE WIT C., ÅSTRÖM K. J. and BRAUN K. (1986): "Adaptive Friction Compensation in DC Motor Drives," IEEE Conference on Robotics and Automation, San Francisco, USA. To appear in IEEE transactions on Robotics and Automation.

[4] ELMQVIST H. (1975): "SIMNON - User's Manual," Report no. 7502, Dept. of Automatic Control, Lund Institute of Technology, Lund, Sweden.

[5] ELMQVIST H., ÅSTRÖM K. J. and SCHÖNTHAL T. S. (1986): "SIMNON - User's Guide for MS-DOS Computers," Dept. of Automatic Control, Lund Institute of Technology, Lund, Sweden.

[6] FRANKLIN G. F., POWELL J. D. and EMAMI-NAEINI A. (1986): *Feedback Control of Dynamic Systems*, Addison-Wesley.

[7] GIBSON J. (1963): *Nonlinear Automatic Control*, McGraw-Hill.

[8] MACSYMA (1983): "MACSYMA Reference Manual," Symbolics Inc., Cambridge, Mass., USA.

[9] SIDMAN M. D. and FRANKLIN G. F. (1986): "Adaptive Control of a Flexible Structure," Proceedings of the 2nd IFAC Workshop on Adaptive Systems in Control and Signal Processing, July 1986. Lund Institute of Technology, Lund, Sweden.

[10] SILJAK D. (1969): *Nonlinear Systems - the Parameter Analysis and Design*, John Wiley & Sons, Inc.

[11] WALLENBORG A. (1987): "Control of Flexible Servo Systems," (Thesis for the degree of Licentiate in Technology) CODEN: LUTFD2/TFRT-3188, Department of Automatic Control, Lund Institute of Technology, Lund, Sweden.